Bull Earthquake Eng (2011) 9:2007–2029
DOI 10.1007/s10518-011-9289-8

ORIGINAL RESEARCH PAPER

Comparison of 3D, 2D and 1D numerical approaches to predict long period earthquake ground motion in the Gubbio plain, Central Italy

Chiara Smerzini · Roberto Paolucci · Marco Stupazzini

Received: 10 November 2010 / Accepted: 25 May 2011 / Published online: 16 June 2011

Abstract In this work we studied the performance of different numerical approaches to simulate the large amplifications of long period earthquake ground motion within the Gubbio plain, a closed-shape intra-mountain alluvial basin of extensional tectonic origin in Central Italy, observed during the Umbria-Marche 1997 seismic sequence. Particularly, referring to the Sep 26 1997 M_w6.0 mainshock, we considered the following numerical approximations: (a) 3D model, including a kinematic model of the extended seismic source, a layered crustal structure, and the basin itself with a simplified homogeneous velocity profile; (b) 2D model of a longitudinal and transversal cross-section of the basin, subject to vertical and oblique incidence of plane waves with time dependence at bedrock obtained by the 3D simulations; (c) 1D model. 3D and 2D numerical simulations were carried out using the spectral element code GeoELSE, exploiting in 3D its implementation in parallel computer architectures. 3D numerical simulations were successful to predict the observed large amplification of ground motion at periods beyond about 1 s, due to the prominent onset of surface waves originated at the southern edge of the basin and propagating northwards. More specifically, the difference of 3D vs 2D results is remarkable, since the latter ones fail to approach such large amplification levels, even when an oblique incidence of plane waves is considered.

Keywords Strong ground motion simulations · Alluvial basins · Complex site effects · Surface waves · High performance computing

1 Introduction

Intra-mountain alluvial basins are a typical surface expression of the extensional tectonic regime that dominates the seismic activity in Central/Southern Italy along the Apennines

C. Smerzini (✉) · R. Paolucci
Department of Structural Engineering, Politecnico di Milano, Milan, Italy
e-mail: csmerzini@stru.polimi.it

M. Stupazzini
Munich RE, Munich, Germany

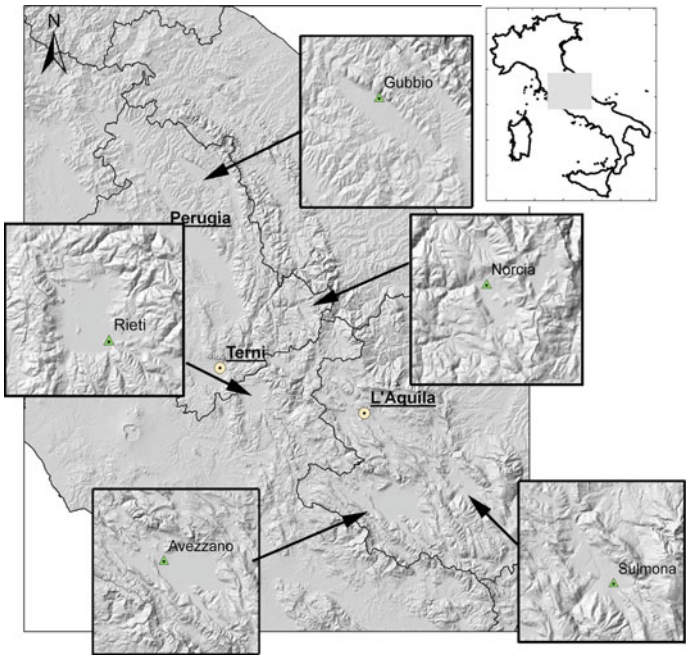

Fig. 1 Examples of closed-shape intra-mountain basins in Central Italy, related to an extensional tectonic regime

chain, as shown by several examples in Fig. 1. A frequent feature of such basins is the relatively small spatial extension (up to few tens of km), their closed-shape and their association to a normal active fault system, capable to produce earthquakes up to magnitude 6.5–7.

Many among the most important Italian earthquakes were originated within normal fault related extensional basins, the last one being the M_w6.3 that devastated L'Aquila and the surrounding villages within the Aterno Valley in Central Italy on Apr 6, 2009, but it is worth recalling as well the M_w7 Marsica earthquake, just about 50 km S of L'Aquila in the Abruzzi region, that devastated Avezzano and the villages surrounding the Fucino plain on Jan 13 1915, causing more than 30,000 deaths, with consequences probably strongly magnified by the basin-induced ground motion amplification.

Several strong motion stations within the ITACA database (ITalian ACcelerometric Archive, http://itaca.mi.ingv.it) are located within such basins and typically show a seismic response exceeding significantly the median spectral ordinates at long periods, calculated by ground motion prediction equations calibrated on the ITACA stations (Bindi et al. 2011).

Standard approaches based on the assumption of vertical propagation of plane waves in horizontally layered media are generally not suitable for earthquake ground motion simulations in such basins, because they cannot account for the wave phenomena arising from the vicinity to the seismic source, such as the polarization of motion related to the focal mechanism, the rupture directivity, and from the complex morphology of the basin, including resonance effects and the basin-edge induced surface wave propagation. A reliable characterization of long period ground motions is of primary relevance for the determination of the seismic demand on large scale structures and oil storage tanks (see e.g. the careful review by Koketsu and Miyage 2008). As a matter of fact, one of the most typical features of seismic

Table 1 List of selected case histories worldwide, where observational evidences of long period ground motions, related to the generation of surface waves within sedimentary basins, have been documented and analyzed with numerical tools. For each case study, the dominant period (T_d) of recorded ground motion inside the basin during the selected earthquake is listed, along with the key references

Basin	Earthquake	M_W	T_d (s)	Key reference
Kanto, Japan	Tonankai 07/12/1944 04:35	8.0	>10–12	Furumura et al. (2008)
Los Angeles, Southern CA	Landers 28/06/1992 11:57	7.2	P2	Wald and Graves (1998)
Los Angeles, Southern CA	Northridge 17/01/1994 12:30	6.7	∼ 2	Graves et al. (1998)
Gubbio, Italy	Umbria-Marche 26/09/1997 09:40	6.0	∼2–3	Pacor et al. (2007), Bindi et al. (2009)
Taipei, Taiwan	Chi-Chi 20/09/1999 17:47	7.6	10–12	Fletcher and Wen (2005)
San Bernardino, Southern CA	Hector Mine 16/10/1999 09:46	7.1	3–8	Graves and Wald (2004)
Yufutsu, Japan	Tokachi-Oki 25/09/2003 19:50	8.3	7–8	Koketsu et al. (2005)
Osaka, Japan	Off Kii Peninsula 05/09/2004 14:57	7.4	5–7	Miyake and Koketsu (2005)
Kanto, Japan	Off Kii Peninsula 05/09/2004 14:57	7.4	7–10	Miyake and Koketsu (2005)
Kanto, Japan	Chuetsu 23/10/2004 08:56	6.6	∼7	Furumura and Hayakawa (2007)

response within such basins is the evidence of prominent contributions of surface waves to long period ground motion, as shown by many examples of strong motion records obtained worldwide within sedimentary basins.

To strengthen this issue, Table 1 provides a selection of research works, illustrating observational evidences of long period ground motions during past earthquakes, related to the generation of surface waves within sedimentary basins. For each case study listed in Table 1, a rough estimate of the dominant period (T_d) of recorded ground motion inside the alluvial basin is also given.

Among the observations of long period amplification obtained at stations of the Italian strong motion network and available in ITACA, the strong motion records obtained inside the Gubbio basin, at station GBP (Gubbio Piana), during the Umbria-Marche seismic sequence, provide the clearest examples of earthquake ground motion within intra-mountain basins in Central Italy. The sequence started on Sep 26, 1997 with two major shocks, the first one at 00:33 GMT, M_W5.7, and the mainshock at 09:40, M_W6.0, both at around 40 km epicentral distance (R_e) from GBP. Figure 2 illustrates the epicentres of the two earthquakes, along with the surface fault projection and slip distribution of the mainshock, after Hernandez et al. (2004).

At GBP, located on soft alluvial sediments, a digital SSA instrument operated between 1991 and 2004 and provided several 3-component records of the Umbria-Marche sequence, while an analog strong motion station (GBB), still in operation, was located at a rock site close to Gubbio downtown, at the Eastern edge of the basin. Location of GBP and GBB stations is also shown in Fig. 2. The most relevant parameters of the records of the main shocks of Sep 26, 1997, at both GBB and GBP are summarized in Table 2.

In Fig. 3 the acceleration records at GBP are shown, together with the record at GBB, for Event 2 alone, since for Event 1 the latter instrument did not trigger. Moreover, GBB

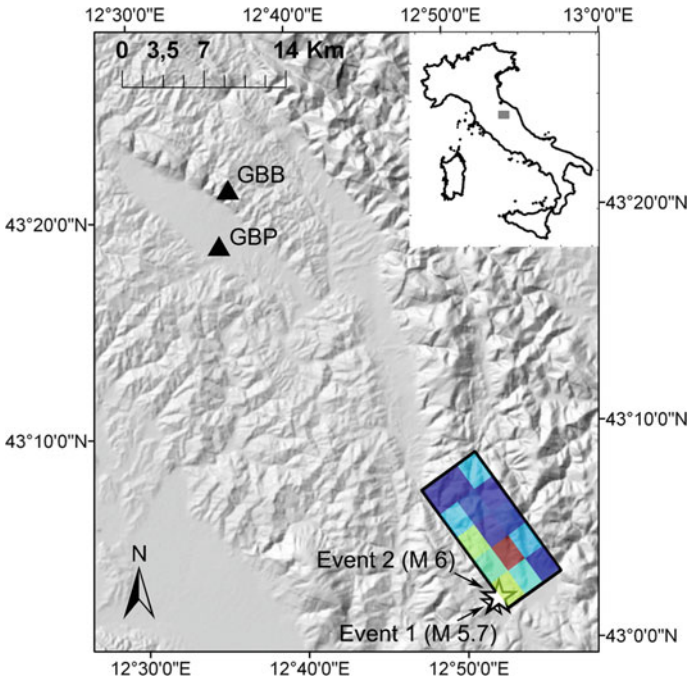

Fig. 2 Digital Elevation Model (DEM) around the Gubbio basin. Triangles denote the Gubbio (GBB) and Gubbio Piana (GBP) stations of the Italian strong motion network. Stars denote the epicenters of the M_W5.7 and M_W6.0 Sept 26 1997 earthquakes (Event 1 and Event 2 in Table 2, respectively) The surface fault projection and slip distribution of Event 2 according to Hernandez et al. (2004) are also shown

late triggered on the S-phase during Event 2, so that it is of limited reliability. In the ITACA database, this record was high-pass filtered at 0.4 Hz, on the horizontal components, and at 0.6 Hz, on the vertical one, so that the spectral ratios involving GBB that will be presented in this paper will be displayed only beyond such corner frequencies. Even accounting for the poor quality of the analog records at GBB, the difference of ground motion at GBB and GBP in terms of duration and frequency content is apparent. Note in Fig. 4 that the 5%-damped acceleration response spectrum of the GBP record, calculated by the geometric average of the horizontal components, lies well beyond the dispersion band of the Ground Motion Prediction Equation (GMPE) calibrated by Bindi et al. (2010), based on Italian data. Comparing the spectrum that would be obtained by windowing the record on the *P*-*S* phase alone, it is also very clear that long period ground motion is amplified by the surface waves propagating within the basin. Further details on strong motion records at stations in Gubbio can be found in Pacor et al. (2007).

After reviewing the available information from recent research activities on the seismic characterization and monitoring of Gubbio basin, the objective of this paper is to study some of the most relevant features of its seismic response at long periods based on different numerical approaches. Namely, we will investigate and compare results of numerical simulations of earthquake ground motion during the Umbria-Marche mainshock (Event 2 in Table 2), from the following numerical models:

Table 2 Strong motion parameters (PGA_h = peak ground horizontal acceleration; PGV_h = peak ground horizontal velocity) associated to GBP and GBB records of the two main events of the Sep 26 1997 Umbria-Marche seismic sequence. Parameters from ITACA: http://itaca.mi.ingv.it. GBB did not trigger during Event 1. R_e denotes the epicentral distance

Event ID	Event Date (time)	M_W	R_e (km)		PGA_h (cm/s^2)		PGV_h (cm/s)		Frequency band (Hz)	
			GBP	GBB	GBP	GBB	GBP	GBB	GBP	GBB
1	26/09/1997 (00:33:12)	5.7	40.57		33.68		3.74		[0.15 30]	
2	26/09/1997 (09:40:25)	6.0	39.57	43.19	95.89	81.65	18.06	2.88	[0.10 35]	[0.4 21] [0.6* 21]

**vertical component*

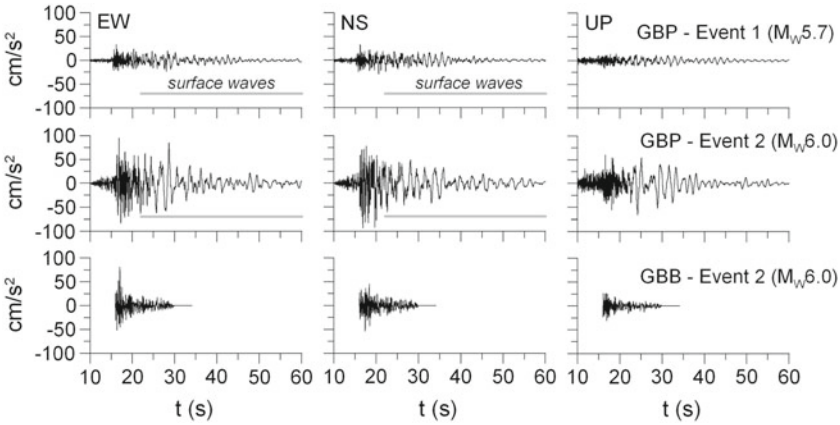

Fig. 3 Acceleration records at GBP for Event 1 and Event 2 (*top rows*), along with records of GBB for Event 2 alone (*bottom row*). The segment of GBP strong motion recordings dominated by surface waves is indicated. Note the late-triggered accelerogram at GBB

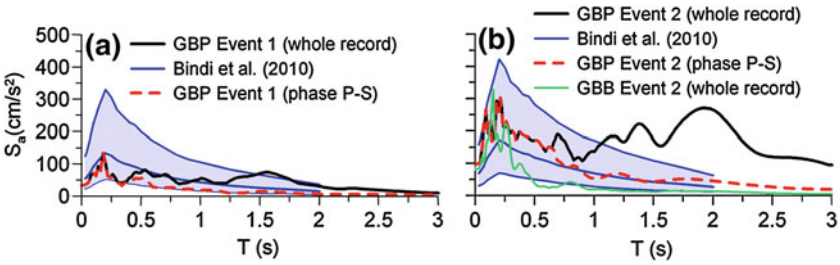

Fig. 4 Acceleration response spectrum, at 5% damping, of the GBP record (*thick black line*), calculated by the geometric average of the horizontal components, compared with the spectrum (*dashed red line*) computed by windowing the GBP record on the P-S phase alone (as pointed out in Fig. 2 by the superimposed segments) for Event 1(**a**) and Event 2(**b**). The spectral accelerations as predicted by the Ground Motion Prediction Equation of Bindi et al. (2010), based on Italian data, is also shown

(a) 3D model of the basin along with a 3D kinematic characterization of the seismic source;
(b) 2D models of longitudinal and transverse cross-sections of the basin under vertical/oblique plane-wave propagation, using, as input, the output of the 3D simulation at outcropping bedrock;
(c) 1D model under vertical plane-wave propagation, using the same input as for point b).

Since one of the main outcomes of this work will be the comparison of results from the different numerical approaches, we will use the same simplified stratigraphy for all models.

2 Simplified seismic characterization of the Gubbio basin

The Gubbio plain, located within a region of shallow extensional seismicity in the Umbria-Marche Appenines, is a 22 km long basin, aligned along the NW-SE directions, with a maximum width of approximately 5 km near the town of Gubbio. The basin is filled by fluvio-lacustrine clayey deposits, with estimated maximum thickness of about 600 m, overlain by superficial alluvial soil layers, mainly consisting of sandy silts and limy clays. The basin is bounded to the east for its entire length by the Gubbio Fault, which emerges at surface in the northern portion of the plain for an observable length of about 30 km. A comprehensive presentation of the geomorphology of the Gubbio plain and its relationship with the seismic activity can be found in Pucci et al. (2003).

The Gubbio basin underwent a comprehensive programme of in-field investigations for its seismic characterization, leading to the estimation of the spatial variability of the depth and dynamic properties of the sediments, by a joint inversion of results of geophysical surveys and microtremor measurements and available borehole V_s measurements. For a thorough presentation of results of such in-field investigation activity, the reader is referred to the Data and Resources section reported by Bindi et al. (2009).

To construct a 3D numerical model of the Gubbio basin, a reasonable balance had to be made between the spatially heterogeneous results from the in-field investigations and the

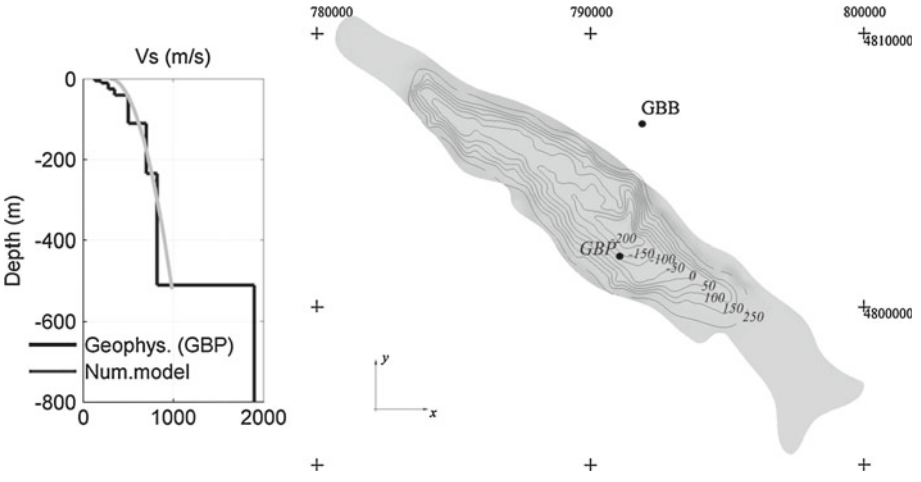

Fig. 5 Left: S-wave velocity profile at valley center from geophysical investigations (*black line*) and the velocity model (Eq. 1) assumed for 3D numerical simulations (*grey line*). Right: Contour lines of the submerged topography of the top of bedrock within Gubbio plain (in meters above the sea level). The location of the strong ground motion acceleration stations of GBP and GBB is also pointed out

practical need to build a numerical mesh as simple as possible, also to reduce the computer time required for 3D simulations. Therefore, a simplified model was defined, considering the submerged bedrock topography illustrated in Fig. 5 and a homogenous average soil profile, expressed as a function of depth z (measured in m from the basin surface) as follows:

$$V_P(z) = 1000 + 30\sqrt{z}; \quad V_S(z) = 250 + 30\sqrt{z}; \quad \rho = 1900 \text{ and } Q_S = 50 \tag{1}$$

where V_P and V_S are the P- and S-wave velocity (in m/s), respectively, ρ is the mass density (in kg/m^3), and Q_S is the S-wave quality factor at 1 Hz.

As noted from Fig. 5, the average velocity profile given by Eq. (1) tends to overestimate locally the V_S values of shallow soil layers, especially in the central part of the basin. However, the influence of such assumption in terms of long period site effects on earthquake ground motion (approximately $T < 1$ s) is negligible and the use of average soil properties is thus justified.

3 Numerical model of the Gubbio basin for 3D seismic wave propagation simulations by the spectral element code GeoELSE

To compare the main features of the seismic response of Gubbio basin under different numerical modelling assumptions, we made reference to the M_W6.0 mainshock of the Umbria-Marche sequence (Event 2 in Table 2). 2D and 3D numerical simulations were carried out by the Spectral Element Method (SEM) software package GeoELSE (*GeoELastodynamics by Spectral Elements*, http://geoelse.stru.polimi.it). To investigate the dependence of results on magnitude, a parametric analysis has been performed by Smerzini (2010), who considered other shocks of the Umbria-Marche sequence recorded at GBP. Preliminary results, still under investigation, show that the dominant period of ground motions, related to the generation of surface waves inside the basin, tends to increase as the earthquake magnitude increases. For the Gubbio case, we found that while the peak spectral amplification is at about 2 s for M6, it decreases to slightly less than 1 s for M5.4 (Smerzini 2010).

The 3D numerical model was constructed by combining the following features: (a) the kinematic seismic source model of Event 2 proposed by Hernandez et al. (2004); (b) the 3D model of the Gubbio alluvial basin as described in the previous section (see Fig. 5 and Eq. 1); (c) a layered deep crustal model; (d) an hexahedral unstructured numerical mesh including both the Gubbio plain and the causative fault; (e) a linear visco-elastic material behaviour with a Q factor proportional to frequency.

GeoELSE is a numerical code for linear and nonlinear wave propagation analyses in heterogeneous media under arbitrary initial and boundary conditions, to simulate a wide variety of problems, such as the seismic response of complex geomorphological structures in near-fault conditions (Stupazzini et al. 2009) or the evaluation of train-induced building vibrations (Paolucci et al. 2003; Paolucci and Spinelli 2006). The code is based on the discretization of the spatial domain by spectral elements, according to the formulation originally introduced by Faccioli et al. (1997) and subsequently by Komatitsch and Vilotte (1998). The implementation of GeoELSE in parallel computer architectures enables one to carry out large-scale numerical simulations of seismic wave propagation in 3D with a reasonable amount of time.

Implementation of a linear visco-elastic soil model in GeoELSE is achieved by a suitable modification of the equations of motion, where the inertial term of the wave equation, $\ddot{u}$, is replaced by an equivalent term, $\ddot{u} + 2\gamma_d \dot{u} + \gamma_d^2 u$, where u is the generic displacement component and γ_d is an attenuation parameter. It can be proved (Kosloff and Kosloff 1986) that such a formulation leads to a frequency dependent quality factor: $Q = Q_0 f/f_0$, where

Table 3 Source parameters used to simulate Event 2. From Hernandez et al. (2004)

Hypocenter (°N, °E, Z)	M_0 (N m)	$L \times W$ (km)	Strike (°)	Dip (°)	Rake (°)	Depth of upper points (km)	Rupture Vel. V_R(km/s)	Rise time τ (s)
43.03°N 12.87°E 5700 m	$1.0\,10^{18}$	12.5×7.5	144	42	270	0.7	2.6	1.0

$Q_0 = \pi f_0/\gamma_d$ is the value at the reference frequency f_0. In our simulations, we adopted $f_0 = 1$ Hz, as a representative value of the frequency range to be propagated.

3.1 Kinematic fault model in GeoELSE

GeoELSE features a number of options that makes it suitable for the kinematic modelling of an arbitrarily complex seismic source. This is enriched by the possibility, on one side, of assigning a realistic distribution of slip along the extended fault plane, as catalogued in the on-line Finite Source Rupture Models Database (Mai 2004) and, on the other side, of defining stochastically correlated source parameters, in terms of rise time, rupture velocity and rake angle across the fault plane. Details of the implementation of such features in GeoELSE can be found in Smerzini (2010).

The source parameters adopted for the kinematic modelling of the Umbria-Marche mainshock (Hernandez et al. 2004) are summarized in Table 3. The numerical model consists of a set of 782 point sources regularly distributed on the fault plane, with spatial discretization corresponding to the nodes of the hexahedral spectral elements in the fault region. Considering about 4 point per minimum wavelength in the spectral element approach, it turns out that the spacing among spectral nodes, and hence point sources, is roughly $\Delta l \sim V_S/4 f_{\max}$, where V_S is the shear wave propagation velocity and $f_{\max}$ is the maximum frequency to be propagated ($\sim$3 Hz). Since $V_R \sim V_S$, V_R being the rupture propagation velocity along the fault, the spacing among point sources governed by grid dispersion criteria, as in this work, turns out to be smaller by a factor of about 2 than that assumed by Hartzell et al. (1978) for modelling a propagating seismic rupture by summation of Green's functions, essentially based on Nyquist sampling criterion. Each point source is activated, starting from the hypocenter, according to the prescribed rupture velocity V_R, with a spatial slip distribution following the Hernandez et al. (2004) model, as shown in Fig. 2. Note that, given the original slip distribution, defined by Hernandez et al. (2004) on a grid of 5×3 subfaults, the use in GeoELSE of a much denser grid of subfaults do not add any information beyond about 1.5 Hz in the source description.

Finally, it is worth noting that the assumption of a constant rupture velocity $V_R = 2.6$ km/s leads to super-shear rupture propagation in specific fault patches, since it is very close or larger than the shear wave velocity of layers B2 and B3 of Table 4, intersecting the fault plane. Such an effect has been addressed by Hernandez et al. (2004) as a realistic possibility. Incidentally, we note that Mai (2004) adopted $V_R = 1.8$ km/s. However, we consider that the main results of our study, essentially concerned with the amplification effects within the Gubbio basin at some 40 km distance from the seismic source, will not be affected by the details of the seismic source kinematic modelling.

Table 4 Layered crustal model, from top (ground surface) to bottom. Adapted from Hernandez et al. (2004) and Mirabella et al. (2004)

Layer #	H (m)	V_P (m/s)	V_S (m/s)	ρ (kg/m^3)	Q_S
B1	1,100	3,500	1,800	2,200	80
B2	1,586	4,000	2,200	2,400	100
B3	1,000	4,800	2,666	2,600	150
B4	3,000	5,500	3,055	2,800	250
B5	–	6,300	3,500	2,900	300

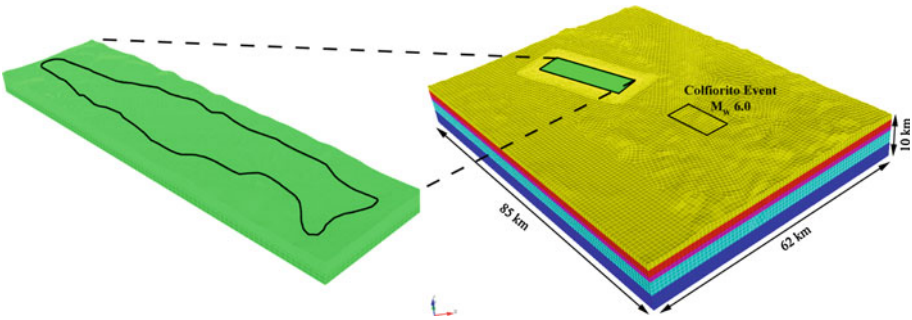

Fig. 6 3D hexahedral spectral element mesh adopted for the computation of the Gubbio case study, with the GeoELSE software package. The surface projection of the seismogenic source (Event 2) considered for the numerical simulations is superimposed and a zoom of the refined mesh around the alluvial basin is given on the *left* hand side

3.2 Spectral element discretization

The 3D spatial discretization by spectral elements of the Gubbio basin and the surrounding area, including the seismogenic source and the layered crustal model specified in Table 4, requires to build up a large-scale unstructured mesh of hexahedral spectral elements. The 3D numerical mesh was obtained thanks to the software CUBIT (http://cubit.sandia.gov) and to the so-called "Not Honoring" (NH) strategy that allows one to construct a 3D numerical grid, based on algorithms of automatic refinement available in CUBIT and easily parallelized (Casarotti et al. 2007), where the bedrock-soil deposit interface is provided as a "soft" constraint. Based on such constraint, GeoELSE automatically associates each node of the SE mesh to either the bedrock or the soil deposit.

The final mesh obtained by the NH strategy is presented in Fig. 6. It consists of 361,752 spectral elements, the size of which ranges from a minimum of about 100 m (inside the basin) up to 900 m. In this way, the mesh can accurately propagate frequencies up to around 3 Hz with spectral degree SD $= 4$, and up to around 2.0 Hz with spectral degree SD $= 3$. This means that within each element there are $(\mathrm{SD}+1)^3 = 125$ or 64 nodes for SD $= 4$ and 3, respectively. The numerical simulations were performed by the Lagrange cluster located at CILEA (http://www.cilea.it/). The main characteristics and the performance of the numerical analyses are summarized in Table 5.

Table 5 3D numerical model size and computational time. Data of CPU time refer to the Lagrange cluster located at CILEA (http://www.cilea.it/)

SD	Elements #	Nodes #	$\Delta t_{simulation}$ (s)	Total simulated time (s)	Total CPU time (64 CPUs) (min)	Set-up time (s)
4	361,752	23,498,665	3.4483×10^{-4}	100	5079 (~84.6 h)	6,136 (~102 min)

4 Numerical results from 3D simulations and comparison with observations

The simulated displacement and velocity time histories and the corresponding Fourier amplitude spectra at GBB, located on gravel breccias at the eastern edge of the basin (left hand side), and at GBP, within the Gubbio plain (right hand side) are compared in Figs. 7 and 8, respectively, with the strong motion observations. Synthetics and observations are both processed with a high-pass acausal Butterworth filter at $f_h = 0.1$ Hz on the three components, for GBP, and at $f_h = 0.4$ Hz on the horizontal components and $f_h = 0.6$ Hz on the vertical one, for GBB. The low pass filter is at $f_l = 3$ Hz in all cases, due to the frequency limitations of simulated results. The record was processed using the procedure described by Paolucci et al. (2010) for similar records in the ITACA database. These comparisons show that there is a reasonable agreement both in time and frequency between simulations and observations, considering the relatively rough modelling of both the source and the propagation path. On the other side, it is worth remarking that numerical model is capable to propagate accurately frequencies up to about 3 Hz, that is a major achievement for this class of numerical analyses, usually limited to a frequency range up to about 0.5–1 Hz. Nonetheless, it is noted that both displacement and velocity waveforms display a stronger decay than the observed ones at frequencies larger than approximately 1.5 Hz. Such rapid decay of spectral amplitudes in this range of frequencies may be reasonably due to the resolution of the slip distribution (see Fig. 2). Since the subfault length of the original slip distribution is $L_f = 2.5$ km (5×3 matrix), the source model will irradiate most energy in the frequency band below approximately $L_f / V_R \sim 1$ Hz, with $V_R = 2.6$ km/s.

As a further check of the successful capability of these 3D numerical simulations to reproduce some of the most salient features of the observed ground motion in the Gubbio basin, we show in Fig. 9 the 5% damped acceleration response spectra obtained through the spectral element code at GBP and GBB compared with the recordings. Superimposed are also the results from some recent GMPEs, namely, Cauzzi and Faccioli (2008) and Bindi et al. (2010). In agreement with the observations, the 3D approach predicts at GBP (left hand side) response spectral amplitudes which exceed remarkably the 84th percentile of the selected GMPEs for periods grater than about 1 s. Strong amplification phenomena, due to the propagation of surface waves generated at the edge of the soft alluvial basin, are particularly evident at $T \sim 2$ s. On the other hand, where the basin amplification effects do not occur such as at GBB, the predictions given by the empirical attenuation laws turn out to be satisfactory. At both GBP and GBB, the underestimation of the numerical simulations at short periods, below about 0.3 s, is due to the frequency limitation of the numerical model, which has been built up to propagate frequency lower than around 3 Hz.

To filter out the possible inaccuracies of the simulated results due to the relatively rough model of the kinematic source and of the propagation path, and to highlight the amplification of ground motion due to the basin effect alone, we have plotted in Fig. 10 the comparison of the recorded and simulated Fourier spectral ratio of GBP with respect to the nearby reference

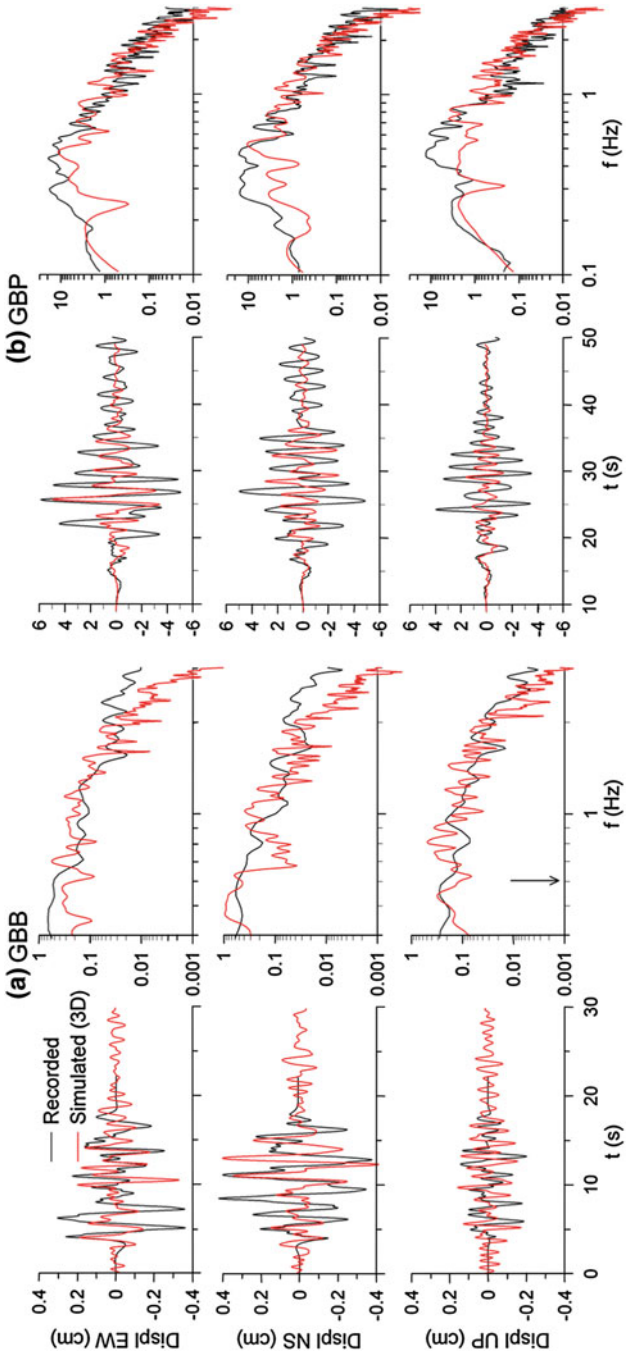

Fig. 7 Comparison of 3D numerical simulation (*red*) by the spectral element code GeoELSE with strong ground motion observations (*black*): displacement time histories (*left*) and corresponding Fourier amplitude spectra (*right*) obtained at: (**a**) GBB and (**b**) GBP. Data are band-pass filtered between 0.4 (except for vertical component: 0.6 Hz as denoted by the *arrow*) and 3.0 Hz for (**a**) and between 0.1 and 3.0 Hz for (**b**)

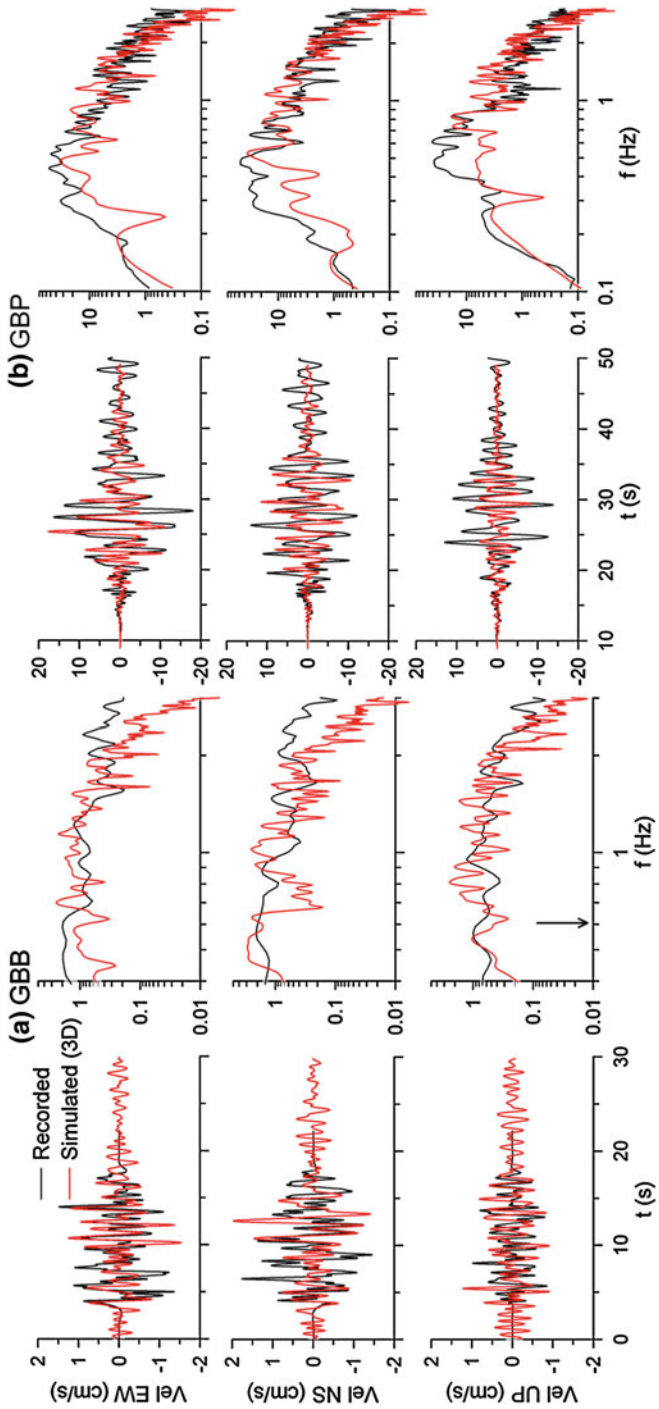

Fig. 8 As in Fig. 7, but in terms of velocity

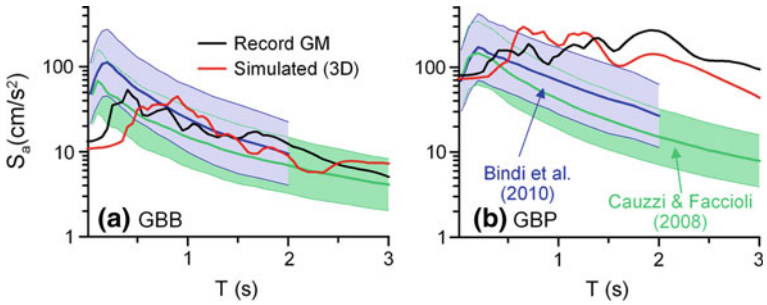

Fig. 9 Acceleration response spectra at 5% damping at GBB (**a**) and GBP (**b**). Comparison of observed values (*black*) with results of 3D numerical simulations (*red*) and predictions by some recent GMPEs. For Cauzzi and Faccioli (2008): R_{hypo} (hypocentral distance) = 42 km and soil class A according to Eurocode 8 ($V_{S30} \geq 800$ m/s) for GBB; $R_{hypo} = 39$ km and soil class C ($180 \leq V_{S30} \leq 360$ m/s) for GBP. For Bindi et al. (2010): R_{JB} (Joyner and Boore distance, i.e. minimum distance from the surface fault projection) = 31 km and soil class $S = 0$ for GBB; $R_{JB} = 27$ km and $S = 2$ for GBP

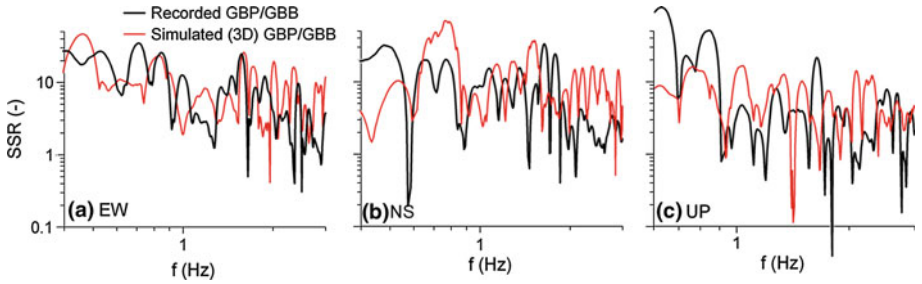

Fig. 10 Comparison between recorded (*black*) and simulated (*red*) Fourier spectral ratios of GBP with respect to the nearby reference rock station GBB (*SSR*), for the EW (**a**), NS (**b**) and UP (**c**) component

rock station GBB, referred to hereafter as Standard Spectral Ratio, i.e., *SSR*, for both the horizontal (a and b) and vertical component (c). Note that data are displayed for frequencies above 0.4 and 0.6 Hz, for the horizontal (a and b) and vertical component (c), respectively, due to the high pass filter applied to the analog GBB recordings (see Table 2). The observed spectral amplification is well predicted, especially at long periods, although some discrepancies in the spectral content between about 0.5 and 0.7 Hz are noted, probably due to the modelling assumptions either on the kinematic source or on the propagation path or on the basin itself.

Finally, 3D numerical simulations provide an interesting insight into seismic wave propagation from the seismic source to the site as well. This is shown in Fig. 11, where some snapshots of the simulated fault parallel velocity component (azimuth = 144°) are plotted. The top panel provides an overview, including the seismic fault, while the bottom panel shows a detailed view of earthquake ground motion inside the Gubbio plain. The snapshots clearly show the onset and propagation of long period surface waves within the basin, once the wavefront reaches its southern edge, with a considerable increase of amplitude and duration of ground motion.

As a further interesting example of how 3D numerical simulations may provide a useful insight into several, often neglected, relevant features of earthquake ground motion, we eval-

uate now the dependence of the 3D Response Spectral Ratios, referred to hereafter as *RSR*s, on the reference ground motion at outcropping bedrock. Although the problems related to choice of a suitable reference ground motion are well known (e.g., Steidl et al. 1996), we aim at showing here the strong dependence of such ratios on the relative position of the reference site with respect to the source and to the basin itself. As an illustrative example, Fig. 12 shows (left hand side) the variability of the *RSR*s computed at GBP, as the geometric mean of the horizontal components, with respect to a set of 12 reference site located at outcropping bedrock (denoted by filled squares on the right hand side map). Specifically, the blue shaded region depicts the 16–84th percentile limits of the *RSR*s computed for the selected suite of reference ground motions. In addition, the *RSR*s of GBP over GBB (*red line*) and over two representative reference sites located at the southern (GBP/S, *black*) and northern (GBP/N, *green*) edge of the basin are superimposed. Note that all *RSR*s were corrected to account for the different source-to-receiver distance. In spite of such correction, considerable period-dependent differences between GBP/N and GBP/S are noted, especially around 2 s, while the *RSR* of GBP/GBB falls within the 16–84th dispersion bands. In general it was found that the *RSR*s with respect to the sites on the Southern edge of the basin are in the lower dispersion band, while the opposite is true for the Northern edge. This means that the wave propagation pattern induced by the presence of the basin has a prevailing role in affecting ground motions at those outcropping rock sites in the shadow zone of the basin with respect to the wave propagation direction.

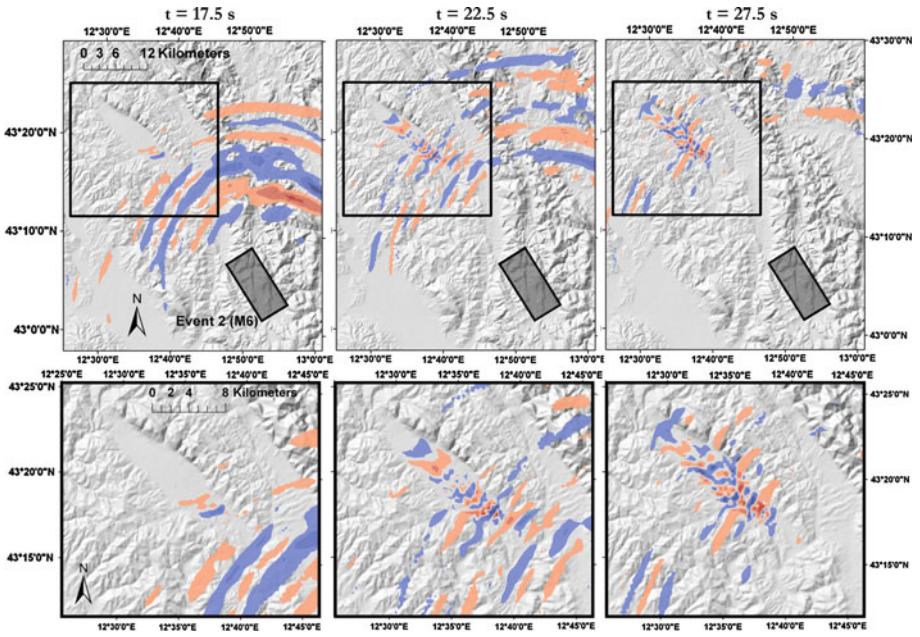

Fig. 11 Snapshots of the fault parallel velocity component (azimuth = 144°) in the Gubbio area obtained with GeoELSE. *Top panel* large view of the Gubbio area including the causative fault of Event 2. *Bottom panel* zoom inside the Gubbio plain, as delimited by the superimposed rectangle in the top panel

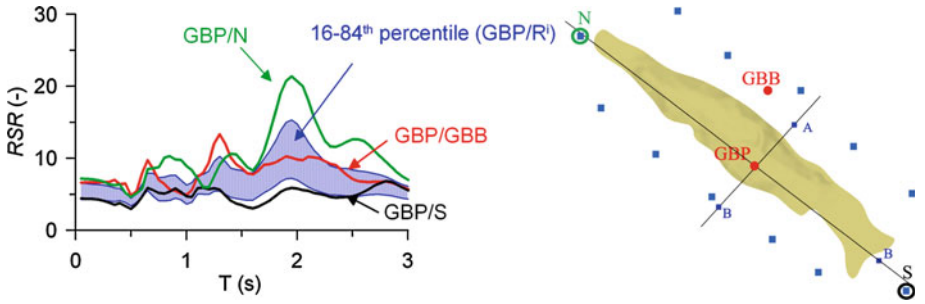

Fig. 12 Dependence of the 3D simulated Response Spectral Ratios (*RSR*s) on reference ground motion at outcropping bedrock, corrected for source-to-receiver distance. The blue shaded region denotes the 16th–84th percentile bands of the *RSR*s (GM, geometric mean) of GBP with respect to a set of 12 reference rock sites (filled squares on the *right* hand side map). In addition, the *RSR*s of GBP over GBB (*red line*) and over two representative reference sites located at the southern (GBP/S, *black*) and northern (GBP/N, *green*) edge of the basin are shown

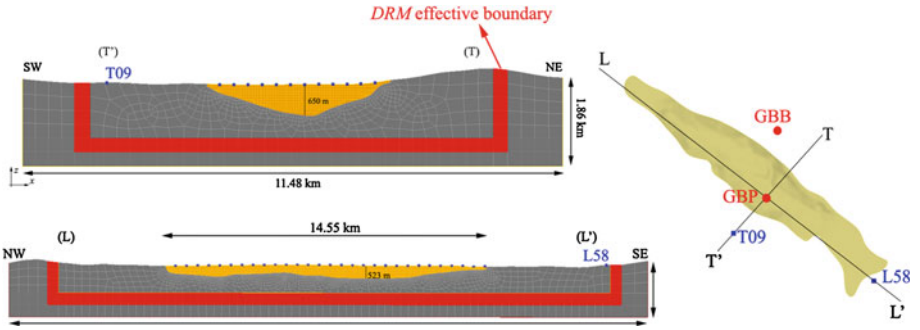

Fig. 13 *Left* 2D numerical models by spectral elements of the transverse (TT′) and longitudinal (LL′) cross-sections of the Gubbio basin. The strip of elements where effective nodal forces are applied according to the DRM approach, is highlighted in red. *Right* location of the TT′ and LL′ cross-sections along with the position of GBP and GBB

5 2D modelling of the seismic response of two cross-sections of Gubbio basin

We aim in this section at making a quantitative evaluation of the performance of 2D models of the Gubbio plain to reproduce the observed long period ground motion and to provide a comprehensive comparison with 3D results.

For this purpose, we started from the same numerical model as used for 3D numerical analyses, and extracted from such model two cross-sections of the basin, the seismic response of which was studied under the hypothesis of both vertical and oblique incidence of plane waves. The surface traces of such cross-sections, aligned on a longitudinal (LL′) and transverse (TT′) axis and passing through the GBP station, are shown in Fig. 13, along with the corresponding numerical grids, discretized by spectral elements.

The oblique incidence plane wave input was implemented in GeoELSE by taking advantage of the Domain Reduction Method (Bielak et al. 2003), that allows one to calculate a set of effective forces applied at a properly selected strip of elements close to the edge of the numerical mesh. Such forces, calculated by solving a wave propagation problem in an *external* domain in free-field conditions, are used as an input to the numerical simulation in the *internal* domain, with the 2D/3D geo-morphological or structural inclusion. In this case,

the effective forces in the external domain are calculated by the classical transfer-matrix approach for vertical/oblique incidence of plane waves in a horizontally stratified soil system (Thomson 1950; Haskell 1953).

When both P and SV wave components are simultaneously present, two independent numerical analyses are carried out and the results are combined, as shown by Smerzini (2010). To clarify this superposition technique, that rigorously applies for linear-elastic behaviour, we denote by U_{SV} and U_P the SV and P in-plane components of motion, respectively, and by $H_{iW}(f)$ the frequency response along the ith direction due to an input harmonic motion of the W type, where W is either SV or P. Following Paolucci (1999), the response at a generic site k can be expressed in the frequency domain as follows:

$$\begin{bmatrix} Y_1(f) \\ Y_2(f) \end{bmatrix}_{(k)} = \begin{bmatrix} H_{1SV}(f) & H_{1P}(f) \\ H_{2SV}(f) & H_{2P}(f) \end{bmatrix}_{(k)} \cdot \begin{bmatrix} U_{SV}(f) \\ U_P(f) \end{bmatrix} \tag{2}$$

where $Y_i(f)$ represents the ith component of ground motion, either horizontal ($i = 1$) or vertical ($i = 2$). $H_{iW}(f)$ is, thus, the transfer function matrix that takes into account the two-dimensional response of the site with respect to plane wave incidence of the W type.

Once each element of the transfer function matrix H_{iW} is known, the 2D response of the model to any multi-component input motion can be easily evaluated. In particular, referring to the case under study, to calculate the response functions $H_{iW}(f)$ at any receiver at surface of the Gubbio basin, two independent numerical simulations by GeoELSE have been performed for both selected cross-sections of the plain. More specifically, the following procedure is followed:

- a Ricker wavelet with maximum frequency $f_{\max} = 3$ Hz (same frequency resolution as in the 3D numerical simulation) and polarized along either the SV or the P component of motion is used as input in two independent numerical simulations;
- from the results obtained with the previous two simulations, for a given receiver, $H_{iW}(f)$ is evaluated as the spectral ratio between the Fourier transform of ground motion along the ith direction due to prescribed SV or P input. For example, the term $H_{2SV}(f)$ is computed as the Fourier spectral ratio of the response along the vertical component (axis 2) over the input Ricker wavelet of SV type.

The seismic response of the two numerical 2D models has been considered under both vertical and oblique plane wave incidence, in the latter case with an angle of incidence with respect to the vertical $\gamma = 20°$. The input time dependence is provided by the 3D numerical simulation at outcropping bedrock. Specifically, we considered receiver T09, for the TT′ cross-sections, and L58 for LL′, after a proper rotation of the horizontal components in the plane of the cross-sections. Location of such receivers is illustrated in Fig. 13.

A comprehensive picture of 2D and 3D numerical results in time domain is given in Figs. 14 and 15, where horizontal in-plane displacements, filtered between 0.05 and 3 Hz, for vertical (left hand side) and oblique (right hand side) plane wave incidence for a set of receivers located along the TT′ and LL′ cross-sections, respectively, are illustrated. It is clear that the contribution of surface waves, generated at the southern edge of the basin and moving northwards with reverberations in the central portion of the plain, is prominent in the 3D results. On the contrary, the presence of surface waves in the 2D case, although clearly apparent especially in the LL′ cross-section subjected to oblique incidence, is significantly less important.

As a further comparison of 2D and 3D numerical results, we illustrate in Fig. 16 the *RSRs* for a set of receivers deployed along the transverse cross-section with respect to the nearby reference station (T09). Acceleration response spectra at 5% damping are considered. It is

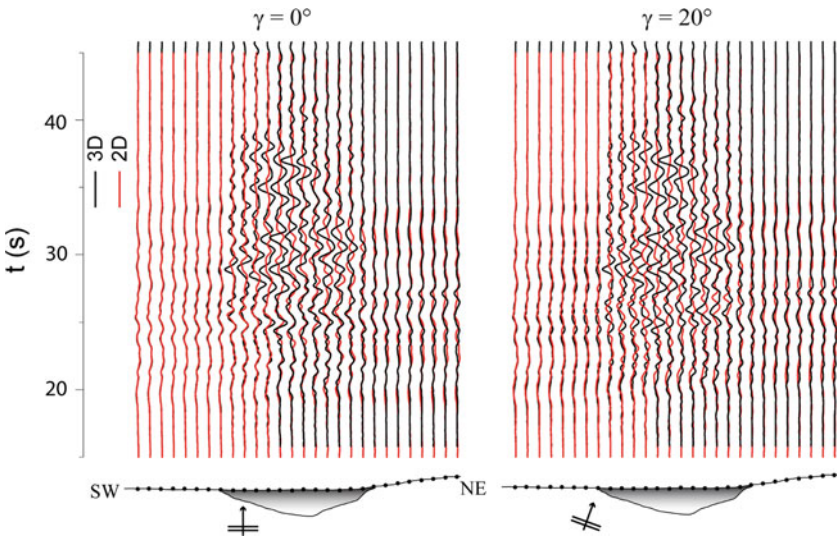

Fig. 14 Displacement time histories at equally spaced receivers located along the transverse (TT′) cross-section of the basin. *Thin black lines* refer to the 3D numerical simulations while *red lines* refer to the 2D model subjected to vertical (*left* hand side) and oblique (*right* hand side) plane waves. For both 3D and 2D models, the horizontal component in the plane of the cross-section is displayed

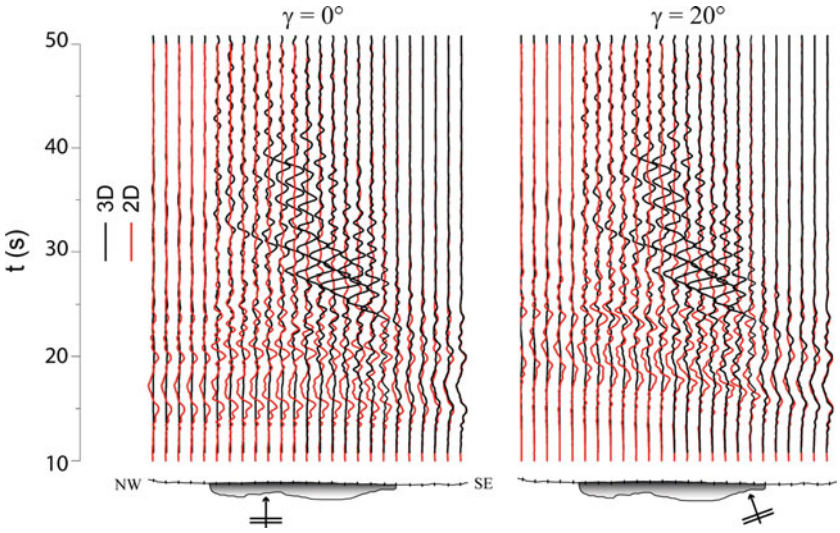

Fig. 15 As in Fig. 14 for the longitudinal (LL′) cross-section of the basin

noted that the 2D vertical plane wave incidence provides levels of response spectral amplification within the Gubbio plain which are strongly underestimated with respect to the 3D case, by a factor of about 4 on average over a fairly broad period range. With the assumption of oblique incidence, the 2D results become closer to the 3D ones, especially in the period range between about 0.5 and 1.0 s. Nevertheless, despite the improvements with respect to

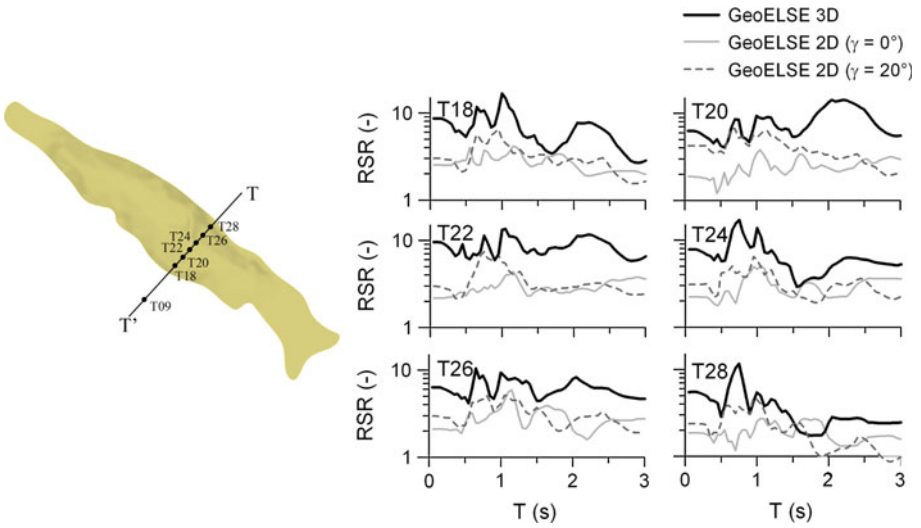

Fig. 16 *RSRs* for a set of receivers located along the TT′ cross-section with respect to the reference receiver located at outcropping bedrock (T09): comparison between 3D (*thick line*) and 2D numerical simulations under vertical (*grey line*) and oblique (*dashed line*) plane wave incidence

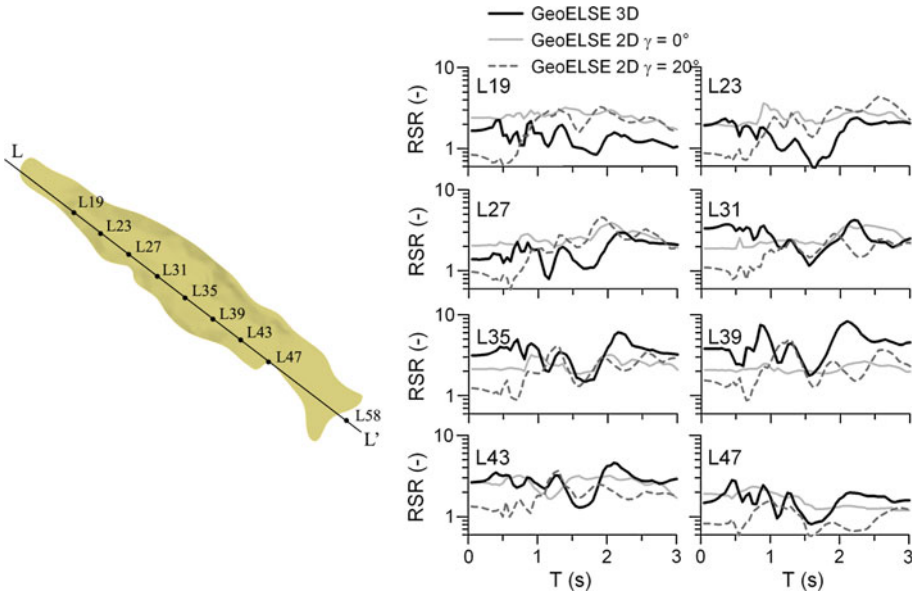

Fig. 17 As in Fig. 16 for the LL′ cross-section. Receiver L58 is used as rock reference site

the assumption of vertical plane waves, the *RSR*s still underestimate the 3D spectral amplifications at long periods ($T > 1$ s).

A similar comparison is depicted in Fig. 17 for the longitudinal cross-section. In this case, 2D and 3D results are closer, especially for oblique incidence, because in this case the 2D configuration approaches the one in 3D. Only on the northern side of the basin (receivers L19 and L23) results tend to diverge, with a significant overestimation of the 2D amplification with respect to the reference site L58.

As a matter of fact, 3D ground motion is more significantly affected by geometric attenuation effects during the northwards propagation. Finally, it is worth noting that close to the valley center (receivers L35 and L39, the latter one corresponding to GBP) the 3D long period amplification significantly exceeds the one in 2D due to the lateral reverberations of surface waves, not present in the 2D model.

6 Comparison of 1D, 2D and 3D numerical results with observed records at GBP

To provide a comprehensive comparison of results from different approaches, we have finally considered the seismic response at GBP site, as calculated by a simple 1D numerical approach. To this end the transfer function for a horizontally layered soil profile with dynamic proprieties defined by Eq. (1) was computed with the classical propagator matrix method for vertical plane wave incidence.

Figure 18 compares the ground motion recordings with the results obtained by 3D, 2D and 1D numerical approaches, both in terms of displacement time histories at GBP and *SSR*s,

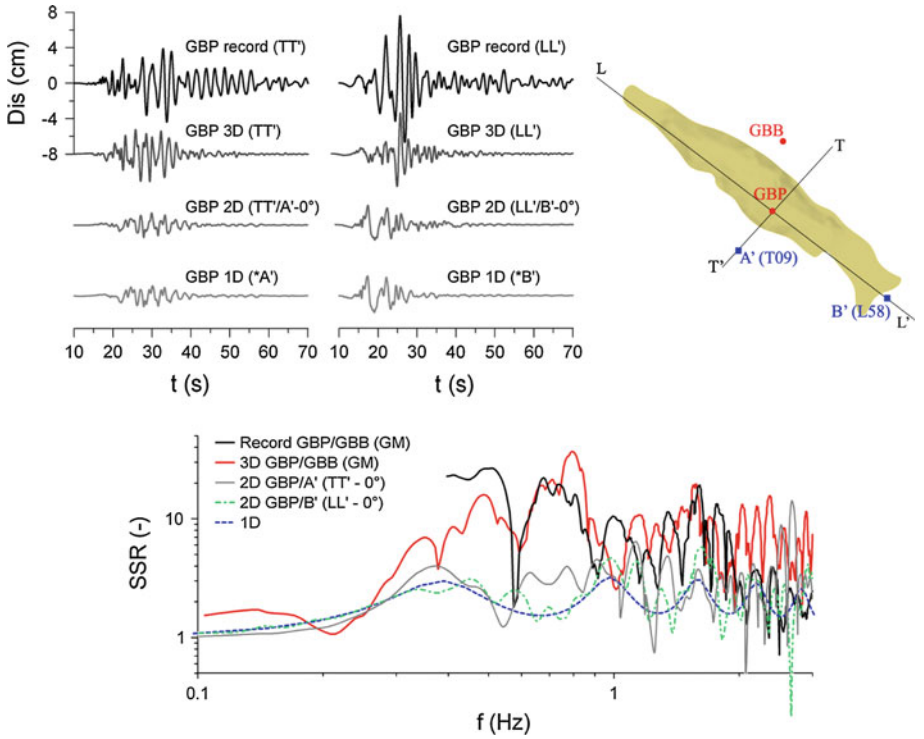

Fig. 18 Comparison of observation at GBP with 3D, 2D and 1D numerical results. *Top* comparison in terms of displacement time histories: recordings and 3D synthetics are rotated along either the TT′ or the LL′ alignments. 2D results are obtained by vertical plane wave incidence using, as input, the output of the 3D simulations at site A′ (T09) and B′ (L58) for the TT′ and LL′ cross-section, respectively. Finally, 1D synthetics have been obtained by convolution of the 1D transfer function with the same input as for the 2D simulations. *Bottom* comparison of recorded *SSR*s of GBP/GBB with those obtained by 3D, 2D (for both TT′ and LL′ cross-section under vertical plane wave incidence, oblique incidence is omitted for sake of clarity) and 1D approaches. The *right top* map shows the location of the reference sites used to compute the *SSR*s

the latter being computed as the Fourier spectrum at GBP divided by the one at a nearby rock reference station. Horizontal components of the observed records and 3D simulations have been rotated along the TT′ and LL′ cross-sections. 2D synthetics are obtained by vertical plane wave incidence, as shown in the previous section. Finally, 1D synthetics have been obtained by convolution of the 1D transfer function with the same input as for the 2D simulations.

Results have been low-pass filtered below a corner frequency of 3 Hz, that is the maximum resolution of the numerical simulations. It is noted that 3D ground motion time histories at GBP approach the observations in terms of amplitude and spectral content, especially when the TT′ component is considered. In contrast, 2D and 1D simulations tend to underestimate significantly the amplitude of the observed ground motion inside the alluvial basin, of at least a factor of 2 in terms of peak values, and are lacking in spectral contributions for frequencies lower than about 1 Hz.

The *SSR*s shown at bottom of Fig. 18 can be regarded as numerical estimates of the amplification function at GBP. Namely, observed and 3D simulated *SSR*s have been calculated as geometric mean of the ratios of the horizontal Fourier spectrum GBP/GBB, while 2D numerical simulations refer to the spectral ratios of GBP over the corresponding reference rock site (T09 or L58). The 1D analytical transfer function, computed as stated above, is also displayed for comparison purposes. For brevity, the results for 2D oblique plane wave incidence are not shown. Note that recorded *SSR*s are not displayed below 0.4 Hz due to the high pass filter applied to the analog GBB recordings.

*SSR*s obtained by 3D simulations show amplifications over a range of frequency between 0.3 and 0.8 Hz in good agreement with observations. On the contrary, 1D and 2D simulations predict a lower and narrower amplification band at around 0.35 Hz, that is the fundamental 1D resonance frequency at GBP. It is interesting to remark that the level of complexity of seismic response introduced by the 3D assumption, but also its adherence to observations, is much higher than in the 1D and 2D cases. As a matter of fact, the contribution of higher 3D vibration modes tends to spread the ground motion amplification over a much broader frequency range than in 1D and 2D. Nevertheless, 2D and 1D simulations provide a better agreement with the observations in the high frequency range, $f > 2$ Hz, where the 3D results estimate larger levels of spectral amplification than those inferred by strong ground motion recordings. This may be due to the frequency-proportional Q factor adopted in our numerical simulations, tending to underestimate the high-frequency amplitude decay, especially within the soft materials of the basin.

Finally, Fig. 19 depicts a similar comparison in terms of *RSR*s. Again, 3D numerical simulations predict spectral amplification factors that are very close to the recorded ones for a period range spanning from about 0.4–2 s. On the other hand, the 1D and 2D approaches provide a strong underestimation of the observed spectral ratios, of a factor of about 4–5 on the entire period range under consideration. It is worth noting that the lack of the SH component and, hence, of Love waves in the 2D model of the Gubbio basin might be a contributing factor to reduce such underestimation, although differences between SH and P-SV results also depend on other factors, such as the frequency content of the input signal and the angle of plane wave incidence (see e.g. Liu et al. 1991; Fishman and Ahmad 1995).

7 Conclusions

This study has shown that the long period amplification observed at GBP station within the Gubbio basin during the 1997 Umbria-Marche seismic sequence is a distinctive feature

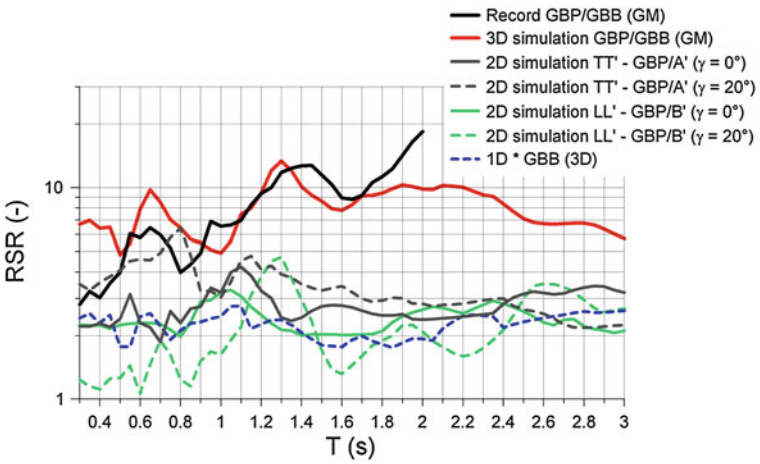

Fig. 19 Comparison between recorded, 3D, 2D (for both TT′ and LL′ cross-section under vertical and oblique plane wave incidence) and 1D *RSR*s computed at GBP station. The reference rock station is either GBB (record, 1D and 3D models) or site A′ and B′ for the TT′ and LL′ cross-section, respectively (see Fig. 18 for further details). GM denotes geometric mean of the horizontal components

related to the onset of surface waves at the southern edge of the basin. The lateral constraint, due to the elongated shape of the basin, traps the surface waves within the basin inducing a large amplification at long periods ($T > 1$ s). Such features have been clearly demonstrated by 3D numerical simulations of earthquake ground motion carried out by the spectral element code GeoELSE, taking advantage of its implementation in parallel computer architectures. At variance with the 3D approach, neither 1D nor 2D numerical simulations were capable to provide such satisfactory results. Therefore, coupling the complex geological configuration of the basin with a realistic kinematic model of the extended seismic fault has been proven to be a successful strategy.

Similar conclusions have been drawn by Olsen et al. (2000), who computed the seismic response of the upper Borrego Valley, Southern California, for a M 4.9 earthquake, for 4th order finite difference 1D, 2.5D and 3D models of the basin. The authors found that both 1D and 2.5D models underestimate of a factor of about 4.2 and 3.5, respectively, the peak ground velocity at main stations on ground surface, especially on the EW component, and fail to predict the duration on all components.

In this work, the successful 3D results were mainly related to the simultaneous presence of two factors, that cannot be properly modelled within a 2D framework, i.e., the markedly 3D shape of the basin, with the sharp concavity at its northern and southern edges, and the location of the seismic source, south of the basin. Studies are presently in progress to check whether similar conclusions could be drawn in the case where the seismic source is located beneath the basin, so to approach more closely the 1D/2D assumptions.

Of course, 3D modelling is not a *panacea* for earthquake ground motion studies, since it is still less reliable than simplified approaches in the high frequency range, especially when local site effect studies are concerned and detailed 1D soil profiles are available. On one side, 3D models have a reduced resolution at high frequency mainly due, on one side, to the computational limitations, related to the size of the numerical domain, and, on the other side, to our limited knowledge on the soil profile at short wavelengths.

In spite of the above limitations, this study has proven the importance of 3D modelling of earthquake ground motion, when the coupling of seismic source and complex site effects plays a dominant role. This is the case of the extensional tectonic depressions advocated in the introductory section of this work, that, as shown by the L'Aquila 2009 earthquake, may experience a dramatic variability of the spatial distribution of ground motion, especially in the near-field of the earthquake, hard to be reproduced by standard approaches for earthquake ground motion prediction. For such cases, 3D numerical simulations may be helpful to produce empirical amplification factors for earthquake ground motions, in a similar way as was previously done for deep basins by Choi et al. (2005) and Day et al. (2008), in the framework of the researches to produce the Next Generation Attenuation (NGA) relationships.

We finally note that non linear effects were neglected for these analyses, since the ground strains induced by the shaking observed in the Gubbio basin during the Umbria-Marche seismic sequence were relatively small. However, the possibility to apply a non-linear elastic constitutive soil model is available in GeoELSE, as shown by the application to the Grenoble Valley case (Stupazzini et al. 2009).

Acknowledgments We deeply thank Ralph Archuleta and Enrico Priolo for the careful review of the manuscript and the thoughtful remarks and criticism that helped improving the paper. This work was carried out in the framework of Project S4 "The Italian strong motion database", funded within the DPC-INGV 2007–2009 Agreement, between the Italian Department of Civil Protection and the Istituto Nazionale di Geofisica e Vulcanologia. Access to supercomputing resources was kindly provided by Consorzio Interuniversitario Lombardo per l'Elaborazione Automatica (CILEA), in Milano. Preliminary work on the seismic characterization of Gubbio basin within Project S3 of the DPC-INGV 2005–2007 agreement, and on the numerical simulations of the Gubbio basin response by Ezio Faccioli and Manuela Vanini, are gratefully acknowledged.

References

Bielak J, Loukakis K, Hisada H, Yoshimura C (2003) Domain reduction method for three-dimensional earthquake modeling in localized regions, part I: theory. Bull Seismol Soc Am 93(2):817–824

Bindi D, Parolai S, Cara F, Di Giulio G, Ferretti G, Luzi L, Monachesi G, Pacor F, Rovelli A (2009) Site amplification observed in the Gubbio basin, Central Italy: hints for lateral propagation effects. Bull Seismol Soc Am 99(2A):741–760

Bindi D, Luzi L, Massa M, Pacor F (2010) Horizontal and vertical ground motion prediction equations derived from the Italian Accelerometric Archive (ITACA). Bull Earthquake Eng 8:1209–1230

Bindi D, Luzi L, Pacor F, Paolucci R (2011) Identification of accelerometric stations in ITACA with anomalous seismic response. Bull Earthquake Eng. This special issue

Casarotti E, Stupazzini M, Lee S, Komatitsch D, Piersanti A, Tromp J (2007) CUBIT and seismic wave propagation based upon the spectral-element method: an advanced unstructured mesher for complex 3D geological media. In: Brewer ML and Marcum D (eds) Proceedings of 1th international meshing roundtable. Springer, New York

Cauzzi C, Faccioli E (2008) Broadband (0.05 to 20 s) prediction of displacement response spectra based on worldwide digital records. J Seismol 12:453–475

Choi Y, Stewart J, Graves R (2005) Empirical model for basin effects accounts for basin depth and source location. Bull Seismol Soc Am 95(4):1412–1427

Day SM, Graves R, Bielak J, Dreger D, Larsen S, Olsen KB, Pitarka A, Ramirez-Guzman L (2008) Model for basin effects on long-period response spectra in Southern California. Earthq Spectra 24:257–277

Faccioli E, Maggio F, Paolucci R, Quarteroni A (1997) 2D and 3D elastic wave propagation by a pseudo-spectral domain decomposition method. J Seismol 1(3):237–251

Fletcher JB, Wen KL (2005) Strong ground motion in the taipei basin from the 1999 Chi-Chi, Taiwan, earthquake. Bull Seismol Soc Am 95(4):1428–1446

Fishman KL, Ahmad S (1995) Seismic response for alluvial valleys subjected to SH, *P* and *SV* waves. Soil Dyn Earthq Eng 14:249–258

Furumura T, Hayakawa T, Nakamura M, Koketsu K, Baba T (2008) Development of Long-period Ground Motions from the Nankai Trough, Japan, Earthquakes: Observations and Computer Simulation of the

1944 Tonankai (M_W 8.1) and the 2004 SE Off-Kii Peninsula (M_W 7.4) Earthquakes. Pure Appl Geophys: 1–23
Furumura T, Hayakawa T (2007) Anomalous propagation of long-period ground motions Recorded in Tokyo during the 23 October 2004 M_W 6.6 Niigata-ken Chuetsu, Japan, Earthquake. Bull Seismol Soc Am 97(3):863–880
Graves RW, Pitarka A, Somerville PG (1998) Ground-motion amplification in the Santa Monica area: effects of shallow basin-edge structure. Bull Seismol Soc Am 88(5):1224–1242
Graves RW, Wald DJ (2004) Observed and simulated ground motions in the San Bernardino basin region for the hector mine, California, earthquake. Bull Seismol Soc Am 94(1):131–146
Hartzell S, Frazier GA, Brune JN (1978) Earthquake modeling in a homogeneous half-space. Bull Seismol Soc Am 68:301–316
Haskell NA (1953) The dispersion of surface waves on multilayered media. Bull Seismol Soc Am 43(1):17
Hernandez B, Cocco M, Cotton F, Stramondo S, Scotti O, CourboulexF Campillo M, Campillo F (2004) Rupture history of the 1997 Umbria-Marche (Central Italy) main shocks from the inversion of GPS, DInSAR and near field strong motion data. Ann Geophys 47:1355–1376
Koketsu KM, Miyage H (2008) A seismological overview of long-period ground motion. J Seismol 12:133–143
Koketsu K, Hatayama K, Furumura T, Ikegami Y, Akiyama S (2005) Damaging long-period ground motions from the 2003 M_W 8.3 Tokachi-oki, Japan, earthquake. Seismol Res Lett 76:67–73
Komatitsch D, Vilotte JP (1998) The spectral element method: an efficient tool to simulate the seismic response of 2D and 3D geological structures. Bull Seismol Soc Am 88:368–392
Kosloff R, Kosloff D (1986) Absorbing boundaries for wave propagation problems. J Comp Phys 63:363–376
Liu SW, Datta SK, Bouden M, Shah AH (1991) Scattering of obliquely incident seismic waves by a cylindrical valley in a layered half-space. Earthq Eng Struct Dyn 20:859–870
Mai M (2004) SRCMOD: online database of finite source rupture models, http://www.seismo.ethz.ch/srcmod/
Mirabella F, Ciaccio MG, Barchi MR, Merlini S (2004) The Gubbio normal fault (Central Italy): geometry, displacement distribution and tectonic evolution. J Struct Geol 26:2233–2249
Miyake H, Koketsu K (2005) Long-period ground motions from a large offshore earthquake: the case of the 2004 off the Kii peninsula earthquake, Japan. Earth Planets Space 57:203–207
Olsen KB, Nigbor R, Konno T (2000) 3D viscoelastic wave propagation in the upper borrego valley, California, constrained by borehole and surface data. Bull Seismol Soc Am 90:134–150
Pacor F, Bindi D, Luzi L, Parolai S, Marzorati S, Monachesi G (2007) Characteristics of strong ground motion data recorded in the Gubbio sedimentary basin (Central Italy). Bull Earthquake Eng 5:27–43
Paolucci R (1999) Numerical evaluation of the effect of cross-coupling of different components of ground motion in site response analyses. Bull Seismol Soc Am 89(4):877–887
Paolucci R, Maffeis A, Scandella L, Stupazzini M, Vanini M (2003) Numerical prediction of low-frequency ground vibrations induced by high-speed trains at Ledsgaard, Sweden. Soil Dyn Earthq Eng 23:425–433
Paolucci R, Spinelli D (2006) Ground motion induced by train passage. ASCE J Eng Mech 132(2):201–210
Paolucci R, Pacor F, Puglia R, Ameri G, Cauzzi C, Massa M (2010) Record processing in ITACA, the new Italian strong-motion database. In: Akkar S et al (ed) Earthquake data in engineering seismology, Chapter 8, Geotechnical, Geological and Earthquake Engineering, 14. Springer, pp 99–113
Pucci S, De Martini M, Pantosti D, Valensise G (2003) Geomorphology of the Gubbio basin (Central Italy): understanding the active tectonics and earthquake potential. Ann Geophys 46(5):837–864
Smerzini C (2010) The earthquake source in numerical modeling of seismic wave propagation in heterogeneous earth's media. PhD thesis, ROSE School, IUSS, Pavia, Italy
Steidl JH, Tumarkin AG, Archuleta RJ (1996) What is a reference site?. Bull Seismol Soc Am 86(6):1733–1748
Stupazzini M, Paolucci R, Igel H (2009) Near-fault earthquake ground motion simulation in the Grenoble Valley by a high-performance spectral element code. Bull Seismol Soc Am 99(1):286–301
Thomson WT (1950) Transmission of elastic waves trough a stratified solid medium. J Appl Phys 21:89–93
Wald DJ, Graves RW (1998) The seismic response of the Los Angeles basin, California. Bull Seismol Soc Am 88(2):337–356